IEEE Access
Multidisciplinary ⋮ Rapid Review ⋮ Open Access Journal

Received 14 August 2022, accepted 1 September 2022, date of publication 6 September 2022, date of current version 15 September 2022.

Digital Object Identifier 10.1109/ACCESS.2022.3204780

RESEARCH ARTICLE

Detecting a Declining Trend of Multidepth Soil Moisture Over the Mongolian Plateau From 1950 to 2020 Using ERA5-Land Reanalysis Datasets

YANGXIAOYUE LIU AND YAPING YANG

State Key Laboratory of Resources and Environmental Information Systems, Institute of Geographic Sciences and Natural Resources Research, Chinese Academy of Sciences, Beijing 100101, China
Jiangsu Center for Collaborative Innovation in Geographical Information Resource Development and Application, Nanjing 210023, China

Corresponding author: Yangxiaoyue Liu (lyxy@lreis.ac.cn)

This work was supported in part by the Comprehensive Survey of Biodiversity over the Mongolian Plateau under Grant 2019FY102001; in part by the Special Program of Network Security and Informatization of the Chinese Academy of Sciences under Grant CASWX2021SF-0106-03; in part by the National Natural Science Foundation of China under Grant 42101475; in part by the Second Tibetan Plateau Scientific Expedition and Research Program under Grant 2019QZKK09; in part by the Branch Center Project of Geography for Resources and Ecology of Knowledge Center, Chinese Engineering Sciences and Technology, under Grant CKCEST-2021-2-10; in part by the National Earth System Science Data Center (http://www.geodata.cn/); and in part by the Capacity Building of Earth System Science Data Center for Chinese Academy of Sciences under Grant WX145XQ07-11.

ABSTRACT Soil moisture (SM) is a pivotal element in surface hydrological processes, energy transfer, and mass exchange over the Mongolian Plateau (MP). However, spatial and temporal SM variability on the MP has remained unclear over previous decades due to global warming. Therefore, we conducted a spatio-temporal investigation of SM in the MP from 1950 to 2020 using ERA5-Land reanalysis datasets. Our research detected a declining trend of SM (from -0.003 m^3/m^3 per decade to -0.005 m^3/m^3 per decade) as well as an increasing trend of soil temperature (ST) (from 0.247 °C per decade to 0.267 °C per decade) along with an increasing soil depth on the MP during the past 70 years. Meanwhile, as the depth increased, the fluctuation degrees of SM and ST gradually declined, and the month for the maximum value emergence was delayed. Statistical analyses, including correlation and Granger causality analysis, suggest that precipitation is the dominant driver of SM dynamics in the MP over the warm season (ST>0 °C). The proportion that precipitation being the cause of the SM variation was above 80% across different depths. Additionally, evaporation is a leading factor in triggering SM fluctuations. The percentage of evaporation being the cause of the SM variation was maintained above 60% among different soil layers over the warm season (ST>0 °C). Meanwhile, multilayer SM, except for the 100–289 cm layer ones, expressed effective feedback to both precipitation (regional proportions varying between 22.64% and 40.28%) and evaporation (regional proportion varying between 36.76% and 64.72%).

INDEX TERMS Soil moisture, the Mongolian plateau, decreasing trend, correlation, causality analysis.

I. INTRODUCTION

Soil moisture (SM) is a key component of the land-atmosphere, water, and energy cycle system [1], [2]. It can efficiently capture and retain the variation characteristics derived from both atmospheric and underground water, which then have a potential influence on the temporal and spatial evolution patterns of climate and ecosystems [3]. Considering the critical role of SM in hydrology, ecology, climatology, meteorology, and agronomy, great efforts have been made to explore and analyze the distribution of SM from various aspects [4]], [5], [6], [7], [8]. Deng *et al.* [9] analyzed the global SM variation trend using the ERA-Interim reanalysis data. They found that the global SM decreased remarkably

The associate editor coordinating the review of this manuscript and approving it for publication was Qingli Li.

during 1979–2017 and will continuously be dominated by a drying trend in the future. Sheffield and Wood [10] conducted research on global drought trends and variability characteristics using SM derived from simulations of the terrestrial hydrological cycle. The results revealed that there was an insignificant wetting trend during 1950–2000 and a drying trend since the 1970s, especially in the high northern latitudes. Albergel *et al.* [11] used three types of reanalysis and remotely sensed SM products to investigate global trend analysis from 1988 to 2010. Two of the three SM datasets (ERA-Land and microwave-retrieved SM) showed a similar declining trend, whereas the MERRA-Land product showed a slight wetting tendency. These studies support the advancement of global SM trend analysis, which could boost our understanding of current hydrological processes in the context of global warming. Despite the overall drying trend derived from the global perspective, the regional SM reveals rather complex conditions owing to the comprehensive effects of climate zones, hydrothermal combinations, underlying surface types, and human activities. Therefore, it is crucial to illustrate the spatial and temporal evolutionary trends of SM at the regional scale to clarify the local SM response to climate change.

The Mongolian Plateau (MP), located in the middle of the Eurasian continent and covering an area of approximately 2 million square kilometers with an average altitude of 1,600 m, has a temperate continental climate. Moreover, the extremely fragile ecology of MP is quite sensitive to global climate change, especially for changes in water availability [12], [13]. Numerous studies have been undertaken on land cover, vegetation, water bodies, and evapotranspiration responses to climate change in the MP [14], [15], [16], [17]. As a sensitive indicator of climate change, long-term serial variation in SM at the MP could be used to distinguish regional climate evolution. Additionally, it could also promote an understanding of the land-surface water cycle and material exchange in the highland areas [5]. Nevertheless, to the best of our knowledge, SM response to climate change on the MP over the past 70 years has rarely been investigated. Hence, it is necessary to disclose the variation features of SM in the MP, which would then be conducive to the understanding of land-surface water storage evolution trends in arid and semi-arid climatic areas. This study will provide a basis for exploring SM variation trends in the MP, while simultaneously determining the interactions between SM and related land-surface parameters (soil temperature (ST), precipitation, and evaporation).

II. STUDY AREA, DATA RESOURCES, AND METHODOLOGY

A. STUDY REGION

As shown in figure 1, the length of the MP is approximately 2500 km East–West and 1500 km North–South. The MP includes the whole territory of Mongolia, the Republic of Tuva, the Republic of Buryat, Transbaikal Krai in the south of Russia, and the north of China's Inner Mongolia Autonomous Region. This plateau falls under the temperate continental climate zone with an annual rainfall of approximately 200 mm and large monthly temperature variations. It has long, cold winters (−23 °C on average) and short, cool summers (16 °C on average). The MP is mountainous in the northwest and dominated by vast bare areas in the southeast and large hills in the middle and east. The altitude gradually decreases from west to east. Influenced by the local climate, the vegetation cover successively spans forests, forest grasslands, typical grasslands, desert grasslands, and Gobi Deserts from north to south.

B. DATA

As the fifth-generation reanalysis product of the European Center for Medium-Range Weather Forecasts (ECMWF), ERA5-Land has attracted extensive attention since its advent. ERA5-Land is produced using 4D-Var data assimilation and model forecasts by the ECMWF. The global ERA5-Land monthly averaged data is published from 1950 to date, with a regular lat–lon grid of 0.1×0.1 degrees. All data can be easily acquired through the Copernicus Climate Change Service Climate Data Store (https://www.ecmwf.int/). The ERA5-Land was developed by combining model data with abundant observations across the globe to formulate a spatial-temporal continuous and consistent climate reanalysis dataset using the laws of physics. The model used in the production of ERA5-Land is the tiled ECMWF scheme for surface exchanges over land, incorporating land surface hydrology (H-TESSEL). For more details about the complicated dynamic physical process of ERA5-Land, readers can refer to [19] and [20]. Four layers of SM and ST are currently available at depths of 0–7 cm (Layer 1), 7–28 cm (Layer 2), 28–100 cm (Layer 3), and 100–289 cm (Layer 4). In addition to ST, precipitation and evaporation are also adopted to explore the underlying process of the cause and effect of SM variation due to their strong interdependence, as proven by various previous studies [8], [21], [22], [23], [24], [25], [26], [27].

In this study, we used monthly ERA5-Land multi-layer SM products from 1950 to 2020 to investigate the soil water content variation characteristics. As the successor of ERA-Interim, ERA5-Land SM products provide various improvements and have been thoroughly evaluated since inception, achieving favorable results compared to other reanalysis products [28], [29]. Although numerous of remotely sensed SM products are available, the prevalently existed gap regions and the limited penetration depth of microwave significantly restrict the comprehensive investigation. Given the penetration limitation of the sensor signal, remotely sensed products can only obtain SM information at 0–5 cm depth. In comparison, the ERA5-Land reanalysis products can retrieve SM information at 0–289 cm depth. Compared to remotely sensed products, ERA5-Land derived SM has notable superiority in terms of spatio-temporal data continuity. Apart from the ERA5-Land SM, the Global Land Data Assimilation System SM is another widely evaluated and used assimilation-based

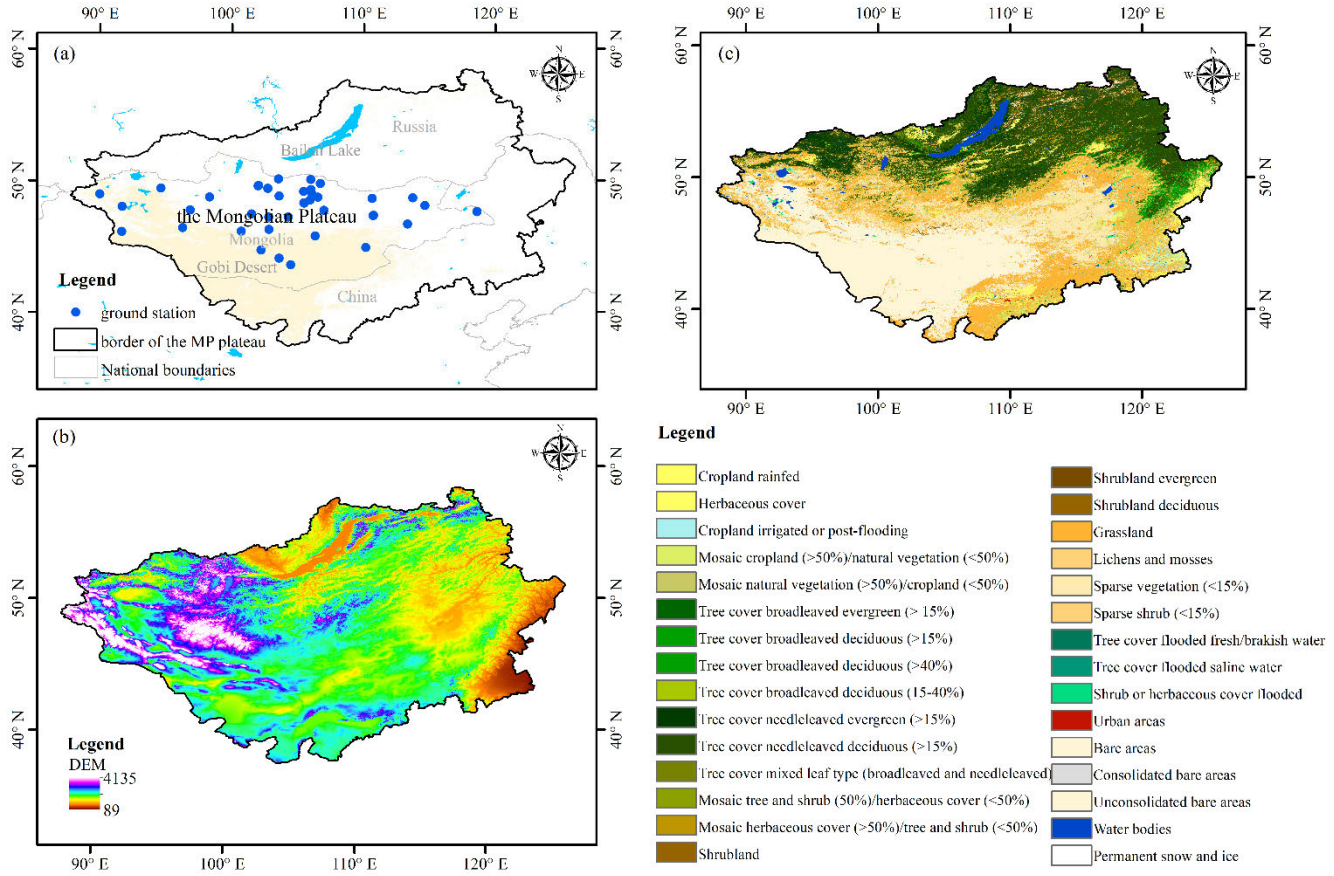

FIGURE 1. **(a) Location of the MP. The border of the MP is derived from the National Earth System Data Center (http://www.geodata.cn/) (b) Digital elevation model of the MP. (c) Land cover types of the MP in 2020. Land cover data were obtained from the European Space Agency Climate Change Initiatives website (https://www.esa-landcover-cci.org/) [18].**

product [30]. Additionally, ST, precipitation, and evaporation were utilized to explore the underlying interactions with SM. Furthermore, the water bodies of the ERA5-Land products in the MP were filtered using the Moderate-resolution Imaging Spectroradiometer (MODIS) 44 w water mask product [31].

The in-situ measurements were downloaded from the International Soil Moisture Network (https://ismn.geo.tuwien.ac.at/en/) to quantitively clarify the accuracy of ERA5-Land SM product over the MP. The MONGOLIA SM ground network had 42 stations, which monitored the soil water content at the depth of 0–0.1 m, 0.1–0.2 m, 0.2–0.3 m, 0.3–0.4 m, 0.4–0.5 m, 0.5–0.6 m, 0.6–0.7 m, 0.7–0.8m, 0.8–0.9 m, and 0.9–1.0 m, individually. And the SM was recorded once every ten days from April to October during 1964–1992.

C. METHODOLOGY

1) PREPROCESSING

The format of ERA5-Land product was transformed from the original NC to TIFF using the programming language Python 3.5 and the Geospatial Data Abstraction Library [32]. Moreover, all the parameters were then converted to the coordinate system of GCS_WGS_1984 to be convenient for subsequent investigations and exhibitions.

The monthly in-situ measurements were achieved by calculating the arithmetic means of the three recordings within one month. Specifically, the monthly value of 0–0.1 m was used as the theoretical true value to evaluate ERA5-Land SM of layer 1; the average value of monthly 0.1–0.2 m and 0.2–0.3 m was applied to verify ERA5-Land SM of layer 2; the average value of monthly 0.3–0.4 m, 0.4–0.5 m, 0.5–0.6 m, 0.6–0.7 m, 0.7–0.8m, 0.8–0.9 m, and 0.9–1.0 m was employed to validate ERA5-Land SM of layer 3.

2) ERROR PARAMETERS

The Pearson correlation (R), bias, root mean square error (RMSE), and unbiased root mean square deviation (ubRMSD) were selected to jointly validate the accuracy level of ERA5-Land SM. Moreover, Previous studies have demonstrated close interactions between ST, evaporation, precipitation, and SM [26], [28], [33]. Thus, the R was also utilized in this study to analyze the degree of their temporal relevance.

$$R = \frac{\sum_{i=1}^{n} (Y_i - Y)\left(X_i - \bar{X}\right)}{\sqrt{\sum_{i=1}^{n} (Y_i - Y)^2}\sqrt{\sum_{i=1}^{n} \left(X_i - \bar{X}\right)^2}} \quad (1)$$

$$Bias = \frac{\sum_{i=1}^{n} X_i - \sum_{i=1}^{n} Y_i}{n} \quad (2)$$

$$RMSE = \sqrt{\frac{\sum_{i=1}^{n} (Y_i - X_i)^2}{n}} \quad (3)$$

$$ubRMSD = \sqrt{\frac{\sum_{i=1}^{n} \left[(X_i - \bar{X}) - (Y_i - \bar{Y})\right]^2}{n}} \quad (4)$$

where X_i and $\bar{X}$ represent the ERA5-Land SM values at pixel i, the arithmetic mean of all the ERA5-Land SM values, Y_i and $\bar{Y}$ represent the in-situ measurements at station i, and the average value of all the in-situ measurements values, respectively.

3) CALCULATION OF THE ROLLING MEAN

The strong seasonality of SM, ST, evaporation, and precipitation could influence the trend analysis and interaction exploration of these variables. Hence, we removed the seasonality of these variables by calculating the rolling mean [34]. The rolling mean equation is as follows:

$$Rolling\ mean\ (t) = S(t - \bar{1}1 : t) \quad (5)$$

where $S(t - \bar{1}1 : t)$ is the average value of the above-mentioned variables d from month $t - 11$ to month t.

4) CROSS-CORRELATION BETWEEN ST, EVAPORATION, PRECIPITATION, AND SM

In an effort to explore the response and memory of SM on ST, evaporation, and precipitation, cross-correlation was used to illustrate the time-series correlation variations [4], [5]. The formula for calculating the cross-correlation is listed in Equation (6).

$$Cross\ correlation = \sum_{n} X\,[n + k] \times Y^*[n] \quad (6)$$

where X is the SM product, Y^* is the complex conjugate of ST, evaporation, or precipitation, n is the n array length, and k is the lag month.

5) GRANGER CAUSALITY ANALYSIS

The Granger causality test was used in this study to explore the coupling relationship between ST, evaporation, precipitation, and SM at corresponding depths. Clive Granger, who won the Nobel Prize in economics as an econometrician in 2003, proposed this test to analyze the causality between variables [35]. This is a statistical hypothesis test for determining whether one time series is useful in forecasting another. The Granger causality analysis has been broadly applied in various fields including economics [36], [37], 38]. In recent years, Granger causality analysis has become increasingly popular in enhancing the understanding of the Earth system science processes [39], [40], [41], 42]. The Granger causality test equations are as follows.

$$Y_t = \sum_{i=1}^{n} a_i Y_{t-i} + \sum_{i=1}^{n} b_i X_{t-i} + \varepsilon_t \quad (7)$$

$$X_t = \sum_{i=1}^{n} c_i X_{t-i} + \sum_{i=1}^{n} d_i Y_{t-i} + \eta_t \quad (8)$$

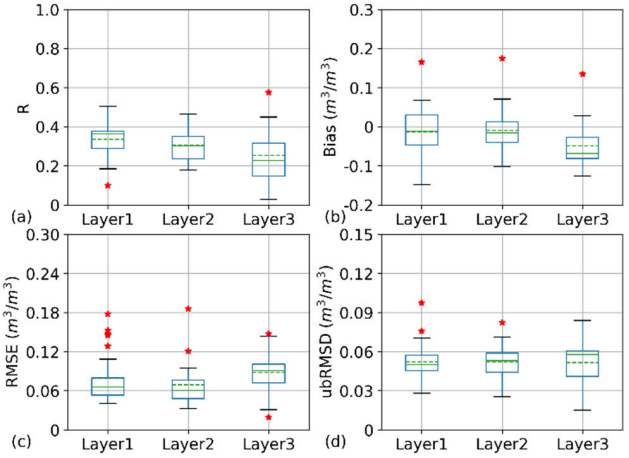

FIGURE 2. Boxplot of R, bias, RMSE, and ubRMSD of monthly ERA5-Land SM at the MONGOLIA network.

TABLE 1. Average values of error parameters of different layers.

Soil layer	Error parameters			
	R	Bias (m^3/m^3)	RMSE (m^3/m^3)	ubRMSD (m^3/m^3)
Layer1	0.33	-0.01	0.08	0.05
Layer2	0.31	-0.01	0.07	0.05
Layer3	0.25	-0.05	0.09	0.05

where X_t and Y_t are two time series, n is the sample capacity, a_i, b_i, c_i, and d_i are regression coefficients, ε_t and η_t are white noise. Equations (7) and (8) demonstrate that the Granger causality test not only considers the interrelationship between the two target variables but also considers the time series autocorrelation in each variable. An F-test was then used to check whether the Granger causality hypothesis is tenable (usually set F≤0.05 or 0.1). If the estimation of Y_t can be significantly improved by taking X_t into consideration compared to merely using past Y_t values, it means that previous values of X_t have a statistically significant effect on the current value of Y_t, and vice versa.

Additionally, a significance test with the confidence level of 95% was used throughout the paper to assure the reliability and stability of our findings.

III. RESULTS

A. ACCURACY VALIDATION

Boxplots were used in this study to display the range of error parameters. The horizontal solid lines from top to bottom represent the maximum, first quartile, median, third quartile, and minimum values [43]. The horizontal dotted line stands for the average, and the red dots indicate potential outliers. As can be seen in figure 2 and table 1, the boxplot revealed an increasing accuracy level as the depth gradually decreased. The Layer 1 SM achieved the superior performance with higher R and smaller bias, RMSE, and ubRMSD.

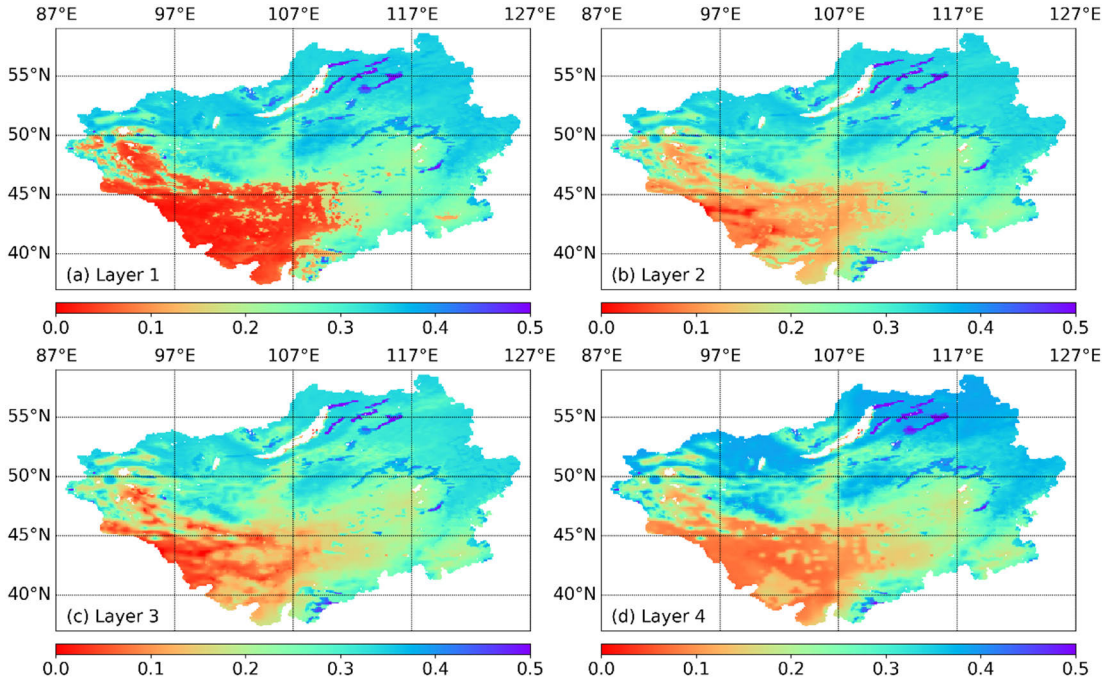

FIGURE 3. Spatial pattern of average SM during 1950–2020 in the MP at different layers. (a) Layer 1: 0–7 cm; (b) Layer 2: 7–28 cm; (c) Layer 3: 28–100 cm; (d) Layer 4: 100–289 cm. (SM unit: m^3/m^3).

The ERA5-Land SM slightly underestimated the in-situ measurements in general. The ERA5-Land SM could basically depict the value of in-situ measurements with low RMSE, ubRMSD, and small bias. Because the monthly mean with only three recordings could hardly express the synthetical condition of SM in a month, the correlations against in-situ measurements were not favorable. And this results was accordant with previous study [28]. Future analysis would be carried out to make further efforts to understand the accuracy of ERA5-Land SM over the TP when daily in-situ measurements are available.

B. SPATIAL PATTERN OF SM AT DIFFERENT LAYERS

Figure 3 shows spatial patterns of the average SM in the MP from 1950 to 2020 at different layers. The dry region ($SM \leq 0.2$ m^3/m^3) is mainly located in the southwest of the MP, which belongs to the Gobi Desert. As one of the largest deserts and semi-deserts in the world, only a small amount of precipitation and few seasonal rivers are surface water supply sources. The scarce water supply combined with prevailing dry north and north-west winds lead to extremely dry conditions. The SM in the Baikal Lake Basin is relatively humid because of the nourishment of the lake and nearby rivers. Apart from soil water extraction, broadly distributed forests and shrublands also play a critical role in SM conservation. Vegetation can effectively redistribute precipitation via interception, absorption, and infiltration. Additionally, vegetation can reduce diurnal temperature differences, ease climate change, and increase air humidity. As a result, the soil remained relatively moist ($SM \geq 0.3$ m^3/m^3).

To intuitively depict the SM pattern variation, we firstly compared the annual average SM values in 1950 and 2020. As shown in figure 4, the SM of all layers became drier in 2020 compared to 1950. The dry regions, shown in red and orange, expanded remarkably from the southwest to the east. Meanwhile, the SM around Baikal Lake Basin remained stable. In addition, cumulative distribution function (CDF) curves were drawn to clearly and quantitatively illustrate a statistical difference in the SM value distribution. As shown in figures 4 (c), (f), (i), and (l), the 2020 CDF curves were much higher during 0.1-0.25 m^3/m^3 than those of 1950, suggesting that there may exist varying degrees of soil water drying trends during the past 70 years. Simultaneously, this integral decreasing variation pattern is roughly consistent with the conclusions of [44], [45]. Considering the extensive variations in SM in the MP, it is important to conduct further analysis to understand specific spatiotemporal evolution characteristics and explore the potential evolutionary mechanisms.

C. TEMPORAL SEQUENCE ANALYSIS

1) TEMPORAL SEQUENCE OF ORIGINAL DATA

The monthly evolutionary sequences of the various SM layers were investigated using scatter density distribution (Figure 5). Every $0.1° \times 0.1$ °C grid inside the MP was treated as scatter in this study. The arithmetic average was also displayed to reflect the overall situation of all scatters. We observed an apparent and regular annual fluctuation cycle of the maximum SM value between the four layers, which could be up

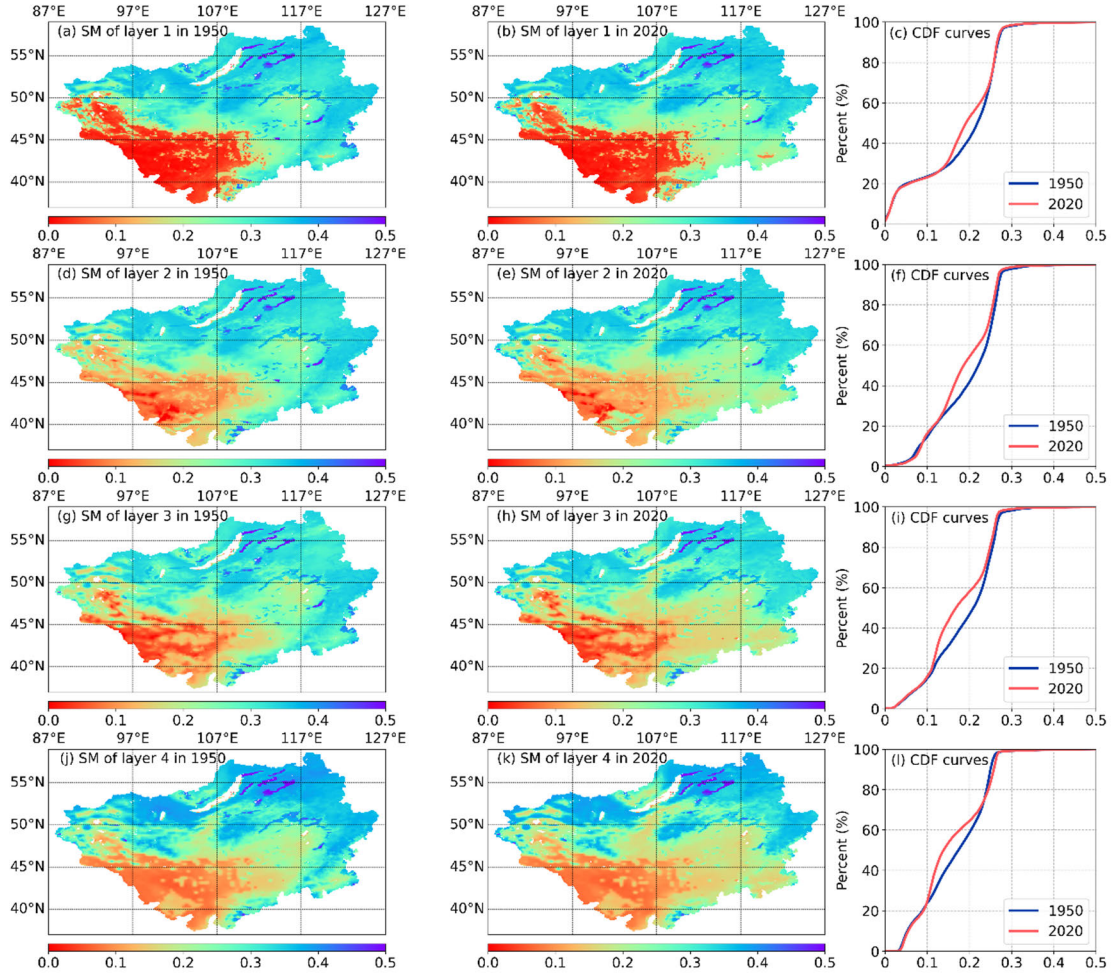

FIGURE 4. Comparison of spatial patterns of annual SM in 1950 and 2020 in the MP at different layers and their corresponding CDF curves. (SM unit: m^3/m^3).

to 0.4 m^3/m^3 in the wet season and down to 0.35 m^3/m^3 in the dry season. However, the minimum value remained stable throughout the year, and the arithmetic average varied between 0.25–0.3 m^3/m^3. In terms of different layers, the SM of layer 4 (at depth of 100–289 cm) exhibited less flow fluctuation than the others, suggesting the relative stability and insusceptibility of the deep layer SM (Figure 5 (d)). Accordingly, as shown in figure 6 (d), the temporal sequences of the deep-layer ST also presented a relatively gentle annual fluctuation trend compared to the other layers. A joint overview of SM and ST showed consistent water–heat covariations in conjunction with the seasonal rhythm cycle. Temporal trends of precipitation and evaporation were also exhibited to describe natural water replenishment and loss conditions (Figures 7 and 8). In figure 8, negative values indicate evaporation and positive values indicate condensation. It can be clearly observed that precipitation and evaporation peaks simultaneously appear in summer. Moreover, SM responded reasonably well to precipitation. Temporary sufficient precipitation can simultaneously enhance the increase of SM and evaporation.

Apart from the long-term temporal sequence, boxplots were drawn to explicitly show the statistical properties as well as monthly variations of SM, ST, precipitation, and evaporation in figures 9–12. As displayed in figure 9, SM was mainly concentrated in 0.18–0.35 m^3/m^3 and the maximum revealed periodic fluctuation except for the layer 4, which was in accordance with the CDF curves in figure 4 and the temporal sequence in figure 5. In terms of ST, there was a pronounced increasing trend with the beginning of summer, and a decreasing trend with the setting in of winter. Moreover, as the soil depth increased, the degree of fluctuation gradually decreased, and a month with the maximum value was delayed. This observation indicated that the influence of air temperature on geothermal temperature can be significantly decreased and delayed by a thick soil layer. Figures 11 and 12 show a significant positive interdependency between precipitation and evaporation. Evaporation could be effectively enhanced by increasing precipitation and temperature. However, there was a gap between precipitation and evaporation, implying that remaining rainfall infiltrated into the soil, leading to a

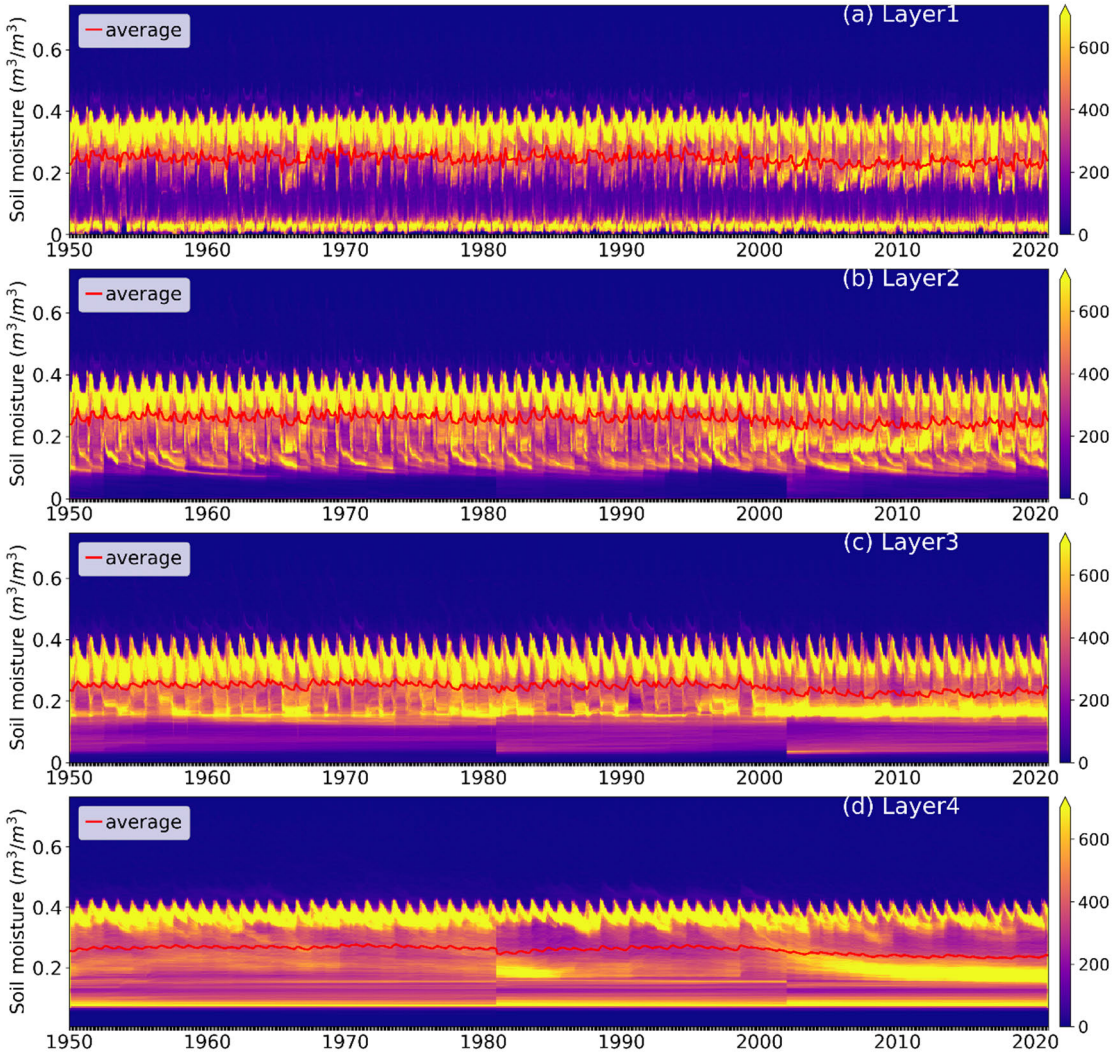

FIGURE 5. Temporal sequences of the original SM scatter density distribution.

gradual increase in SM from the surface layer to the bottom layer.

2) ROLLING MEAN TREND ANALYSIS

To explore the integral trend, rather than merely focusing on the seasonal cycle, the long-term mean seasonal variation was removed from each parameter by subtracting the moving average of the preceding 12-month. The rolling mean characteristics of SM, ST, precipitation, and evaporation are plotted with confidence intervals (Figures 13–16). Trends in the time series were investigated using linear regression. A statistically significant negative trend of [-0.003, -0.005] m^3/m^3 per decade was found for SM. This decreasing trend was aggravated by increasing soil depth. This phenomenon indicated that although the deep layers behaved relatively impervious to seasonal climatic changes, the climate elements did have a significant impact on the long-term evolutionary trend of the deep layer compared to the surface layer SM. Correspondingly, as shown in figure 14 (a)–(d), this finding could also be supported by the increasing trend of ST. There was a 0.247 °C per decade positive trend for layer 1, and a 0.267 °C for layer 4, outlining an 8 % increase compared to layer 1. Additionally, precipitation revealed a slow decreasing trend of -0.016 mm per decade, and evaporation exhibited a similar trend of 0.005 mm per decade. It can be observed that there was a gap between the decrease of rainfall and evaporation. This gap meant that SM and root absorption did not correlate with decreasing precipitation. Overall, it was indicated that SM reduces as depth increases, and this trend might be triggered by the combined action of increasing temperature and decreasing precipitation. The impact of precipitation on the surface layer SM declination was verified in a previous study using both remotely sensed and reanalysis products [45].

D. SPATIAL TREND ANALYSIS

1) CORRELATION ANALYSIS

ST, precipitation, and evaporation are important parameters that exhibit bidirectional interactive responses to SM. When temperature increases, water evaporates from the soil to the air, resulting in a decrease in soil water content [27], [46].

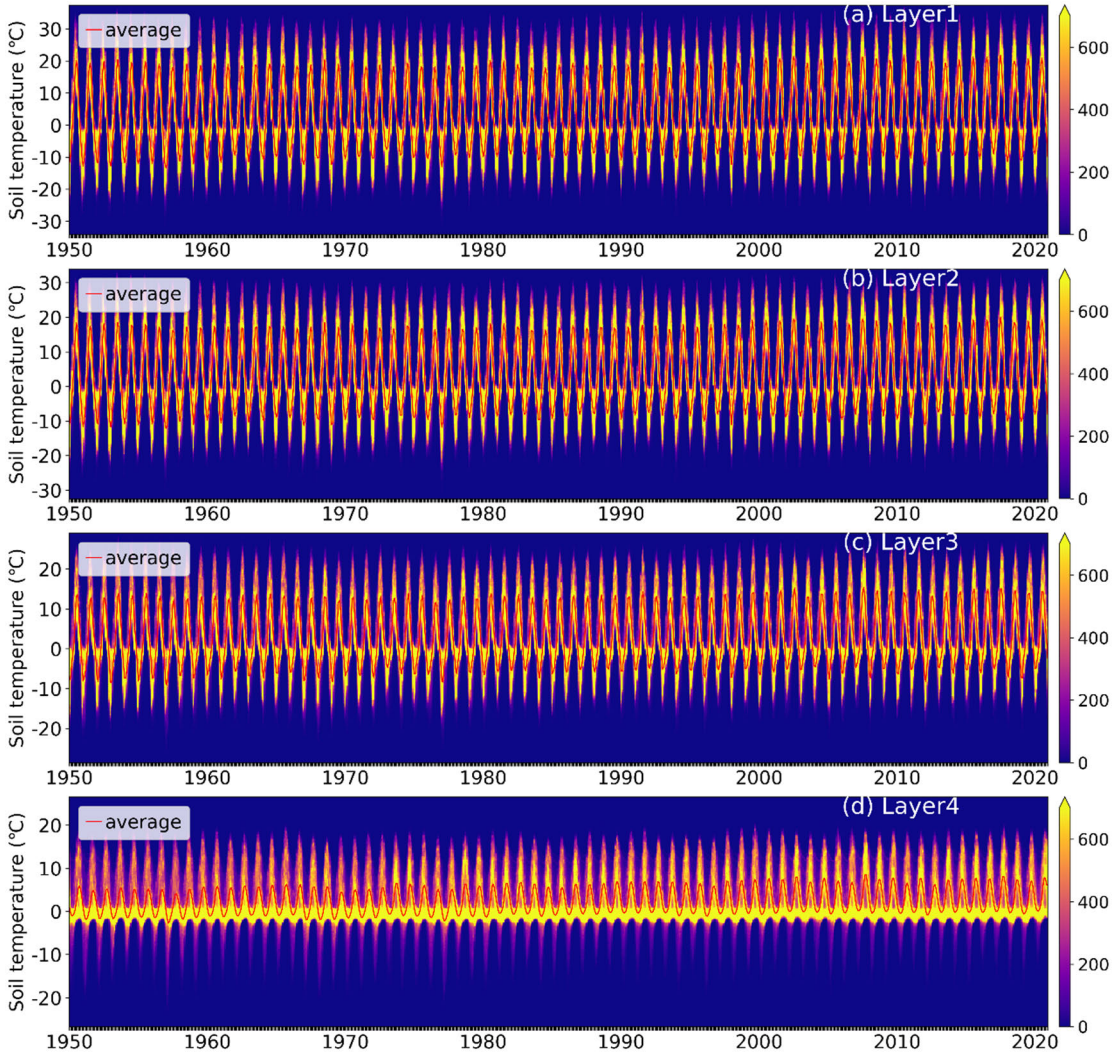

FIGURE 6. Temporal sequences of the original ST scatter density distribution.

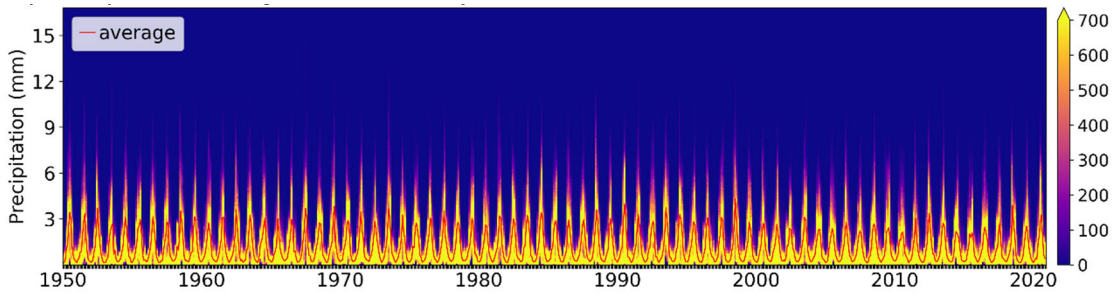

FIGURE 7. Temporal sequence of the original precipitation scatter density distribution.

Meanwhile, owing to the high specific heat capacity, water vapor could effectively absorb air heat, thereby reducing the temperature. The temperature and moisture gaps between the soil and air is then reduced, and the evaporation process also reduced. SM is responsive to precipitation, and the effect of precipitation on SM has been demonstrated by various researchers [21], [33], [47]. Additionally, positive and negative SM-precipitation feedback in terms of regional aridity have been reported [8], [23], [48].

Figure 17 displays the density scatterplots between the different SM layers and the above-mentioned parameters on the MP. Despite the different depths, the SM of the four layers

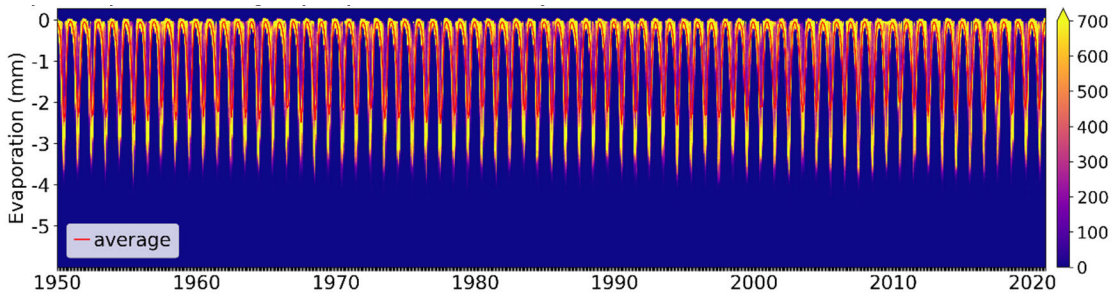

FIGURE 8. Temporal sequence of the original evaporation scatter density distribution.

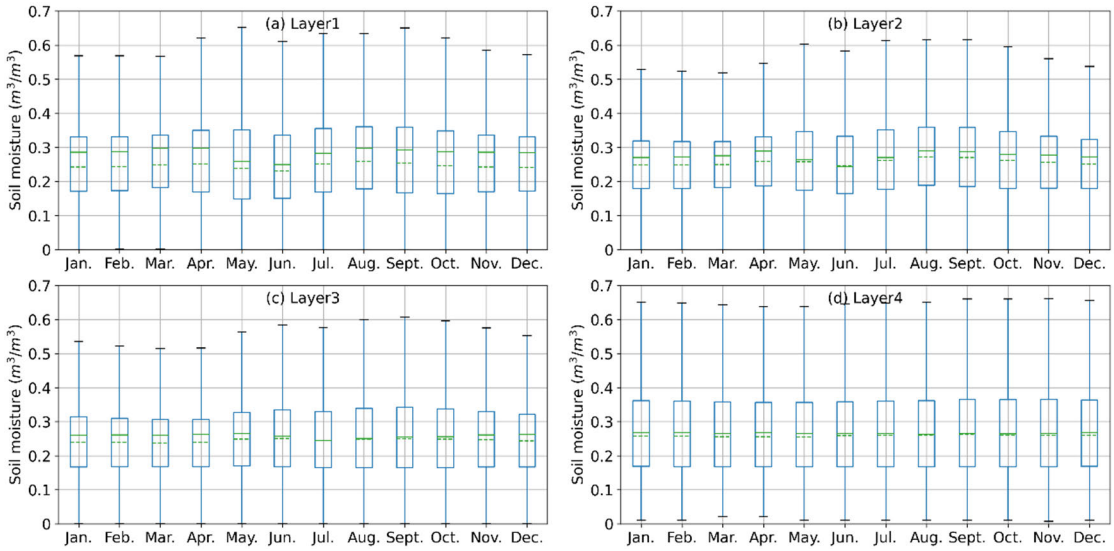

FIGURE 9. Monthly SM averages for different layers during 1950–2020.

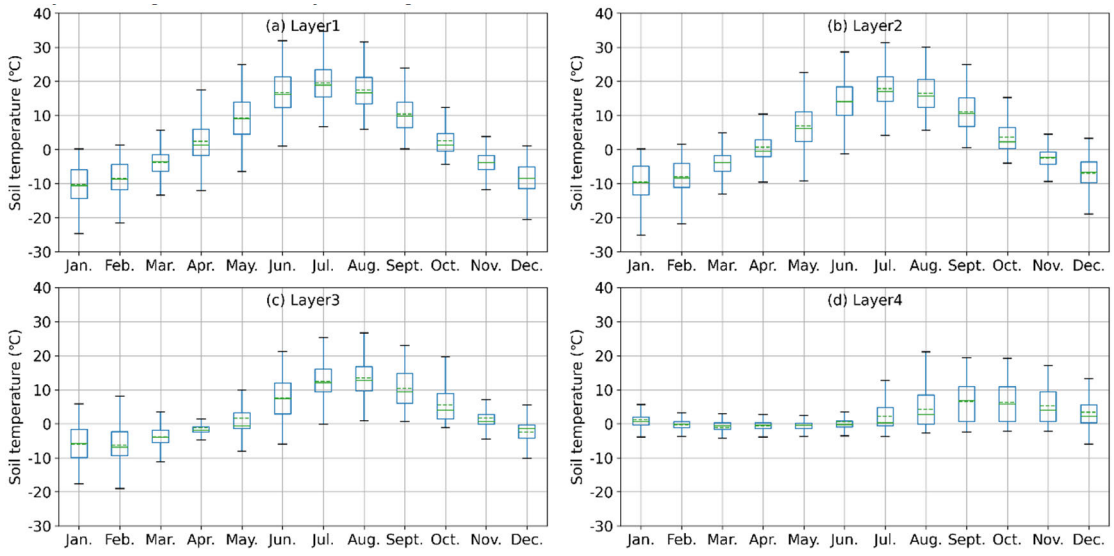

FIGURE 10. Monthly ST averages for different layers during 1950–2020.

responded relatively similar to the corresponding parameters. As can be seen from figure 17 (a)–(d), there was a negative correlation between SM and ST, which is in accordance with widely acknowledged findings [28], [49]. Similarly, we observed a significant positive correlation between precipitation and SM. It was noticed that when SM was around

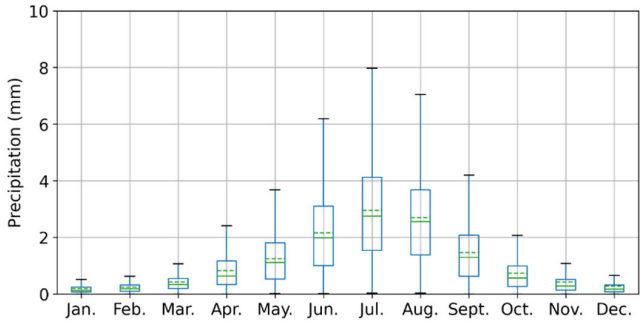

FIGURE 11. Monthly precipitation averages during 1950–2020.

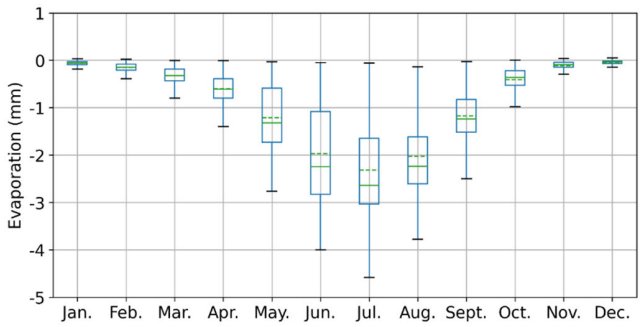

FIGURE 12. Monthly evaporation averages during 1950–2020.

0.35 m^3/m^3, the increase in precipitation could remarkably promoted the increase of SM, suggesting that the soil reaches the saturation threshold. In terms of water loss, evaporation increased with increasing SM. However, the evaporation gradually decreased when SM steadily exceeded 0.35 m^3/m^3, which could have resulted from reduced energy availability linked to rainy or cold periods.

In addition to the simple density scatterplot discussion, it is equally meaningful to analyze the time lag of the increasing depth of SM in response to the promoting or restraining effects of ST, precipitation, and evaporation. The rate of heat conduction, rainfall infiltration, and water evaporation can be influenced by soil depth, soil texture, land cover, and topography. This suggests that there may be different lags with increasing depth. The temporal cross-correlations between ST, precipitation, evaporation, and SM are shown in figure 18. As illustrated in figure 18 (a)–(d), ST revealed decreasing effects on SM with increasing depth. In comparison, it can be observed from figure 18 (e)–(l) that both precipitation and evaporation displayed almost the same cross correlation to different layers of SM, which were not affected by soil depth. The cross correlations usually achieved the maximum values in the current month, indicating that the influence derived from ST, precipitation, and evaporation could spread to the SM from 0 to 289 cm depth within one month.

2) SPATIAL EVOLUTIONARY DISTRIBUTION AND CAUSAL LINK ANALYSIS

Figure 19 shows spatial trend patterns of the different SM layers from January 1950 to December 2020. The significance of the trend was set at $p < 0.05$. Over 70% of the region presented a decreasing trend across various depths, with the largest drop occurring in the southeastern and central parts of the MP (rendered in red). Furthermore, the deep SM layer displayed a more severe degree of drought variation than the shallow layers. In contrast, less than 30% of the area revealed a slightly increasing trend, which was mainly distributed along the northeastern as well as northwestern borders of the MP (rendered in purple). Simultaneously, precipitation expressed a corresponding reducing pattern where the SM decreased and an insignificant increasing trend where the SM also turned wet (Figure 21). Accordingly, evaporation demonstrated a coincident evolution pattern to precipitation, increasing at the point where the precipitation increased (Figure 21). Nevertheless, it appears that the ST pattern was not closely linked with the overall SM trend, implying that temperature might not be the dominant element that triggered SM fluctuation. Even so, it is noteworthy that the ST deep-layer presented a more significant warming trend than the surface layers. Only regions around Lake Baikal remained relatively stable, highlighting the efficient capability of the water body in regional heat regulation among various soil depths.

The possible causality between the different SM layers and related parameters was explored using Granger analysis. As shown in figure 23(a)–(d), areas without significant casual links were prevalently distributed in the MP, indicating an inconspicuous interaction between SM and ST. Nevertheless, it is worth noting that the percentage of ST was found to be the unidirectional cause of SM increase from 12% to over 50%, expanding from west to east, with a gradual increase in the soil depth. In terms of precipitation, significant unidirectional causality relationships appeared in over 50% of the MP areas across all the layers (Figure 23(e)–(h)), illustrating a detectable impact of rainfall on the promotion of SM. Furthermore, in terms of the first three layers, SM and precipitation were found to have evident bidirectional causality relationships, which accounted for 21.52%, 39.78%, and 30.05% of the MP, respectively. While for the fourth layer, the percentage of bidirectional causality sharply dropped to 10.56%, implying that it could be difficult for SM at 100–289 cm or deeper to have a significant effect on precipitation. For evaporation, significant bidirectional causality relationships between SM and evaporation gradually declined as soil depth increased (Figure 23(i)–(l)). Furthermore, the evaporation was stably maintained to have a far-reaching impact on every layer of SM. SM also presented an evident decreasing effect on evaporation with increasing soil depth. Besides, since ERA5-Land considers both the liquid and solid water content, ERA5-Land SM remains nearly constant over the frozen season. Therefore, precipitation and evaporation could hardly impact SM when ST $< 0\,^{\circ}C$, and substantial influences from precipitation and evaporation are mainly concentrated over the warm season.

IV. DISCUSSION

SM has long been considered a critical indicator for characterizing land-surface hydrological evolution and climate change

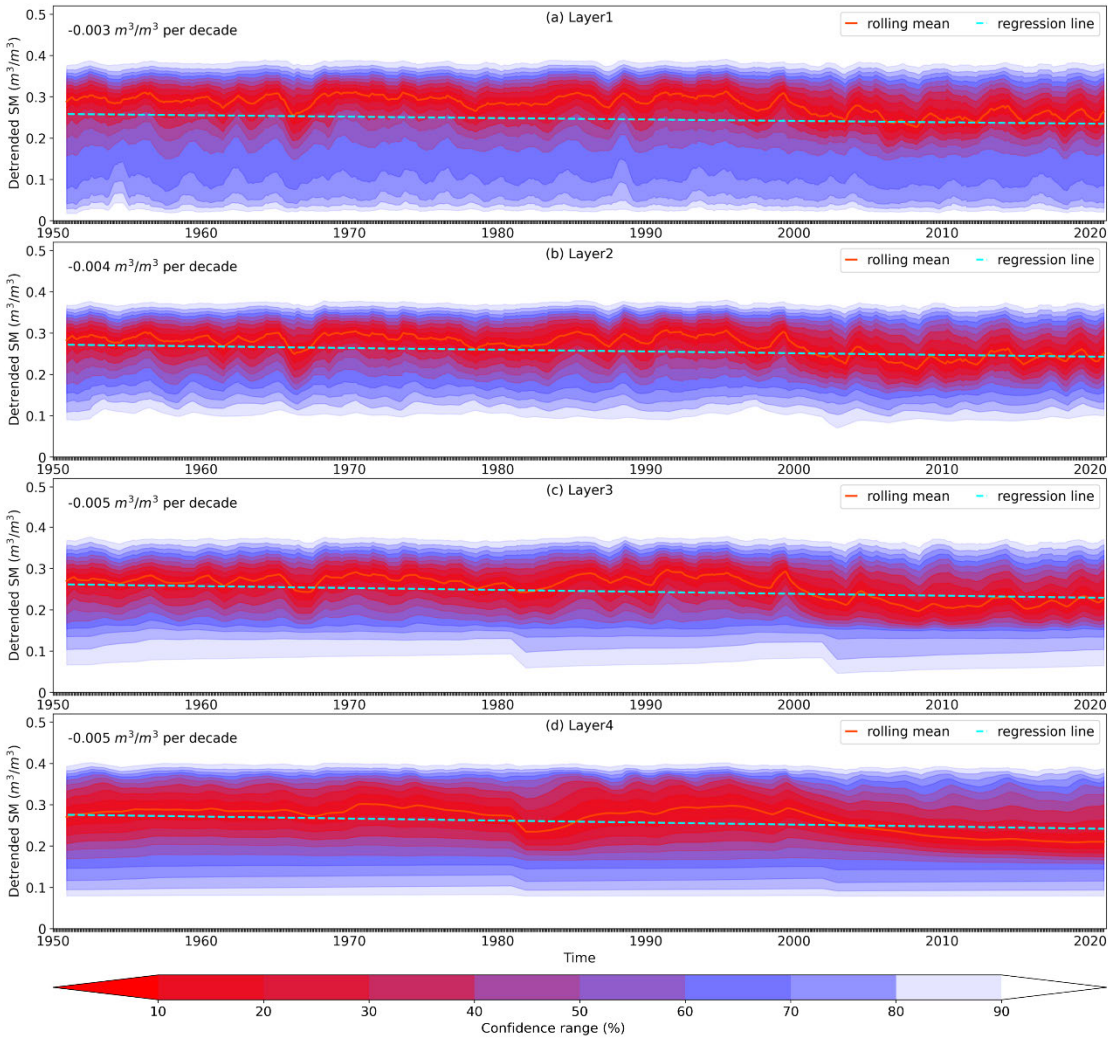

FIGURE 13. Monthly SM rolling mean (red line) and regression line (cyan line) for different layers during 1950–2020. Gradient shading represents the confidence intervals for the SM ensemble.

trends [44], [50]. Multi-layer SM derived from ERA5-Land has been widely evaluated and utilized since its inception [28], [29], 30]. This study systematically investigated long-term SM evolution trends in the MP from 1950 to 2020. A conspicuous loss trend was detected among all the available layers.

A. SM VERTICAL VARIABILITY PATTERN

During the analysis process, we firstly identified that the SM became wetter with increasing depth in the arid and semi-arid areas of the MP, which is called the inverse humidity phenomenon [51]. According to previous studies [52], [53], depth is the dominant source of heterogeneity in the volumetric SM content. Atmospheric water can be transformed into soil water through condensation (including distinct types of precipitation) and infiltration. When precipitation occurs, rain infiltrates the soil pores and replenishes the soil water content. The SM surface layer quickly increased and then gradually declined. Accordingly, the deep soil layer is nourished by the transferred moisture. Then, the SM and groundwater are transformed into each other through infiltration and evaporation. SM enters the atmosphere through evaporation (vegetation transpiration) and is transformed into atmospheric water. Soil evaporation is usually divided into atmosphere-controlled, soil hydraulic conductivity-controlled, and diffusion-dominant stages in terms of the declining soil evaporation rate [54].

In addition to the wetting trend in the vertical direction, SM exhibited a stable trend with increasing soil depth. The seasonal fluctuation of SM gradually decreased as the soil depth increased, implying that deep-layer SM could be impervious to seasonal climate rhythms. During the downward transportation of water through soil pores, soil layers intercepted a portion of the water, less water is obtained, and a smaller amplitude was exhibited as the depth increases [55]. Meanwhile, the surface SM was highly variable owing to the direct and synthetic influence of atmospheric conditions. Moreover, the corresponding ST also presented a

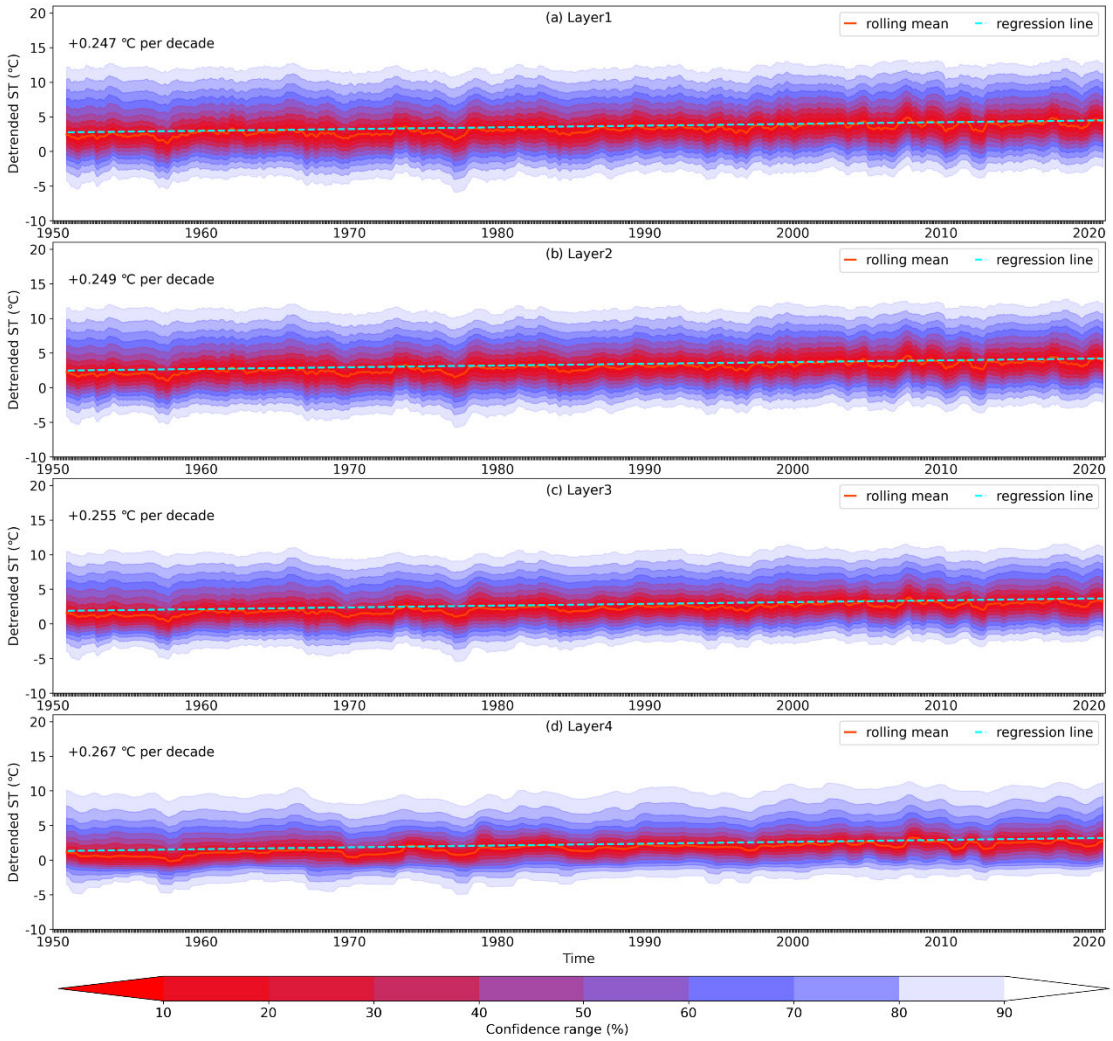

FIGURE 14. Monthly ST rolling mean (red line) and regression line (cyan line) for different layers during 1950–2020. Gradient shading represents the confidence intervals for the ST ensemble.

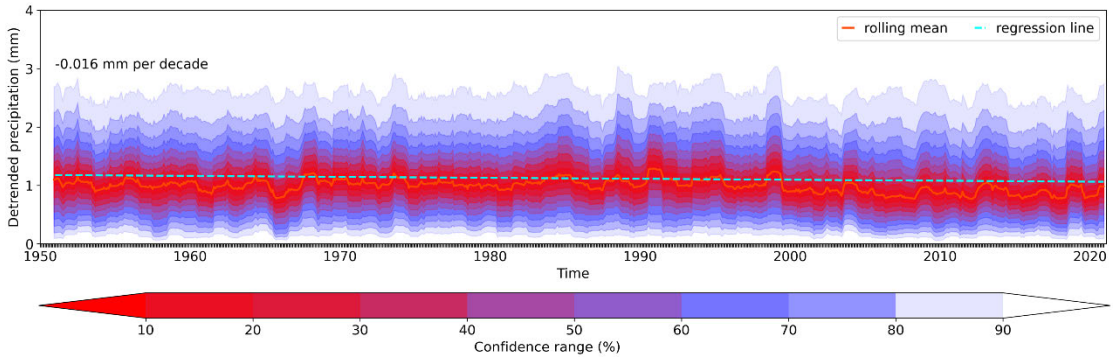

FIGURE 15. Monthly precipitation rolling mean (red line) and regression line (cyan line) during 1950–2020. Gradient shading represents confidence intervals for the precipitation ensemble.

similar stability tendency, and the fourth-layer ST showed mild yearly variations compared to the others. Additionally, the month in which the maximum occurred gradually displayed the latency feature with increasing soil depth. The month with the peak temperature could be delayed from July (first layer) to August (fourth layer). This pattern correlated roughly with previous investigations based on reanalysis and satellite-derived datasets [11], [28], [56], [57]. In addition,

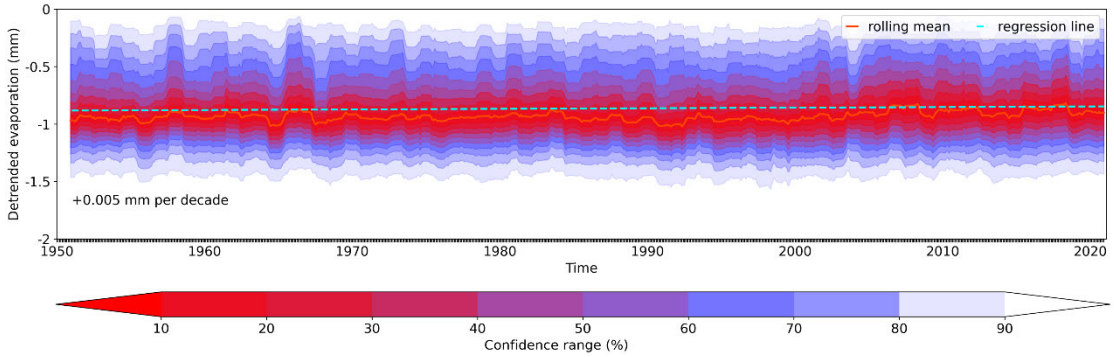

FIGURE 16. Monthly evaporation rolling mean (red line) and regression line (cyan line) during 1950–2020. The gradient shading represents the confidence intervals for the evaporation ensemble.

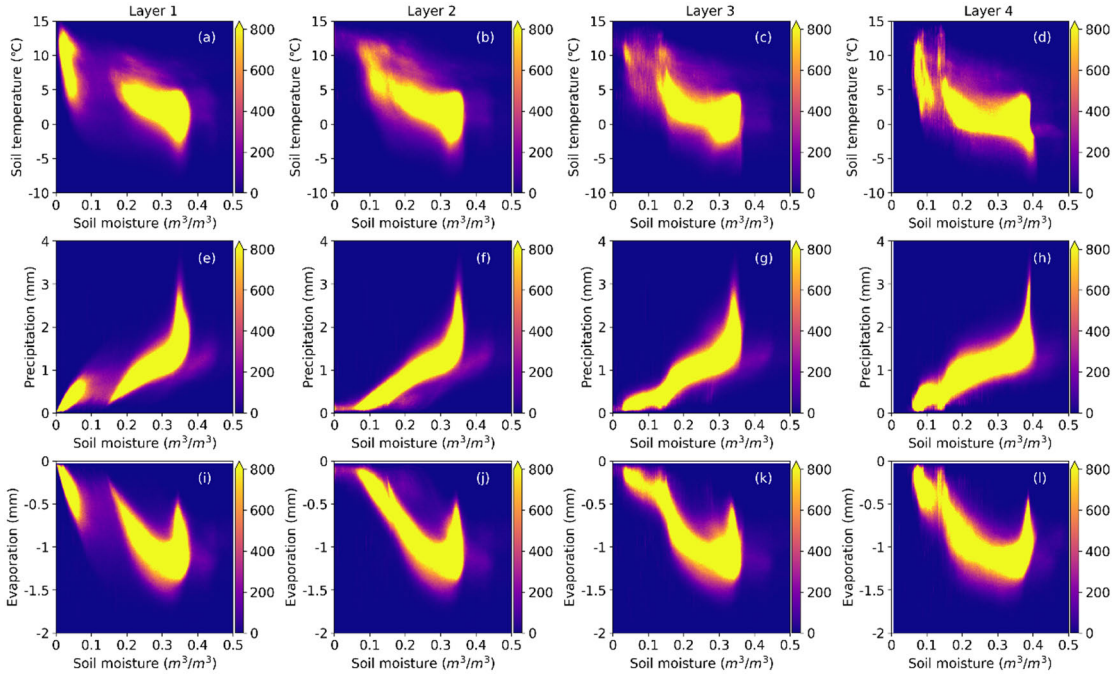

FIGURE 17. Scatter density plot between different layers ST ((a)–(d)), precipitation ((e)–(h)), evaporation ((i)–(l)), and the corresponding SM.

as previously reported [58], for all conditions of surface SM observations across the globe, the variability in surface-layer SM could be larger than that in the root-zone. This revealed that surface-layer variability can be reduced when extreme dry conditions are considered [23].

B. ATTRIBUTION ANALYSIS

Through comprehensive investigations, this study primarily concluded that the SM on the MP has undergone continuous declination over the past 70 years. The drying trend intensified as soil depth increased. Furthermore, there was a gradual increase in the ST warming with increasing soil depth. Both precipitation and evaporation showed an overall decreasing tendency. This conclusion is supported by a previous study [45]. This study assessed remotely sensed and reanalyzed SM in the MP and indicated that surface SM exhibited a decreasing trend during the warm season for the period 1982–2018. Precipitation played a more significant role than temperature in explaining the dynamic trend of SM, as reported by the partial correlation analysis. Meng *et al.* [44] conducted a quantitative assessment of SM spatiotemporal variability in the MP from 1982 to 2019 and demonstrated a significant decreasing trend in SM. The SM dynamics are mainly induced by precipitation and potential evapotranspiration.

To further explore the potential correlation between the dynamics of SM and related atmospheric conditions, this study provides a preliminary analysis of the interactions between these parameters using the Granger causality test. The precipitation was identified as the vital Granger cause of SM in over 80% of the MP across different layers, demonstrating the predominant influence of precipitation events on SM dynamics. Conversely, SM at 0–100 cm depth was

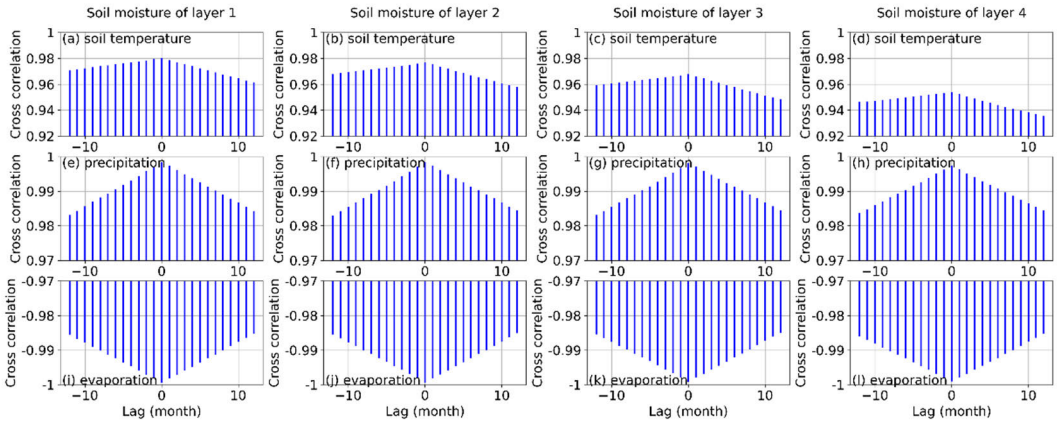

FIGURE 18. Cross-correlation between different layers ST ((a)–(d)), precipitation ((e)–(h)), evaporation ((i)–(l)), and the corresponding SM.

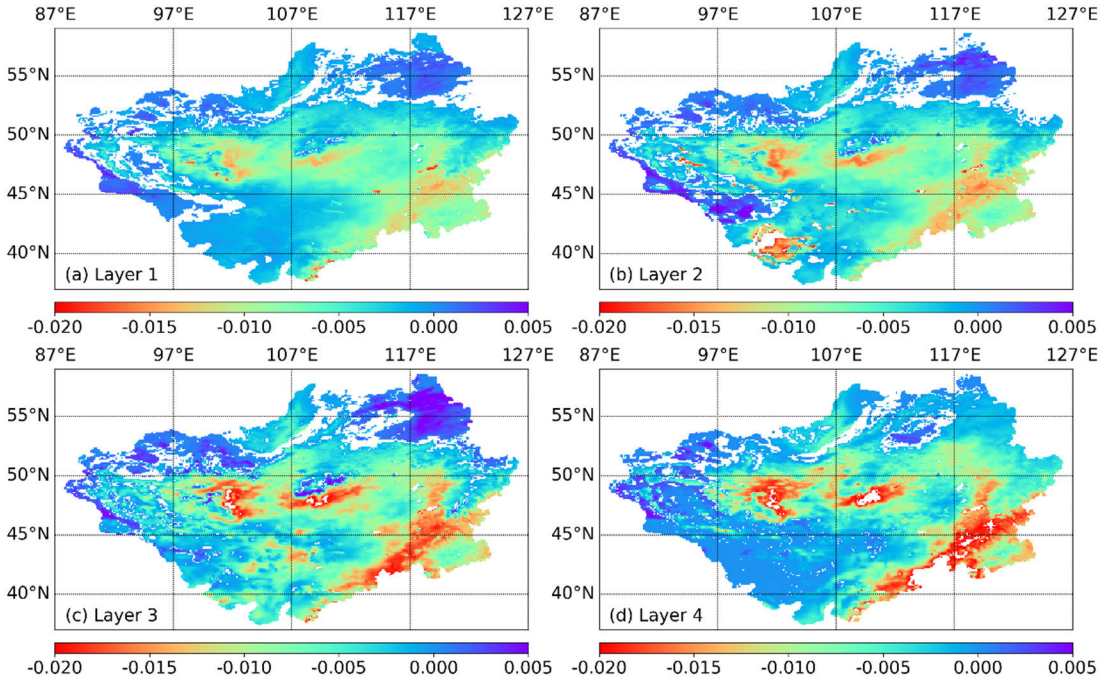

FIGURE 19. Spatial evolutionary trend of different SM layers on the MP. Areas without significant trends are shown in white.

detected to be the Granger cause of precipitation in 21.52%–39.78% of the MP. On the one hand, it is well acknowledged that precipitation can efficiently enhance an increase of SM. On the other hand, SM has been proven to have various impacts on precipitation probabilities in terms of regional aridity [23]. The specific mechanism of SM and precipitation interaction is a complex process involving atmospheric conditions, land surface moisture, boundary layer, and wind speed. Besides, evaporation was thought to be the Granger cause of SM in over 60% of the MP, whereas the impact of SM on evaporation gradually declined as the depth increased. Simultaneously, the SM-evaporation feedback was not significant at high latitudes, where the energy available for evaporation was small [26]. Moreover, the proportion of ST that could be speculated to be the Granger cause of SM increased with increasing depth. According to a previous investigation [59], the increase in SM (in this study, the SM increased as the depth increased) could result in a higher heat storage capacity, which effectively reduces the irregular fluctuation of the ST originating from unpredictable atmospheric conditions. Thus, the water–heat covariations in the soil could be physically consistent.

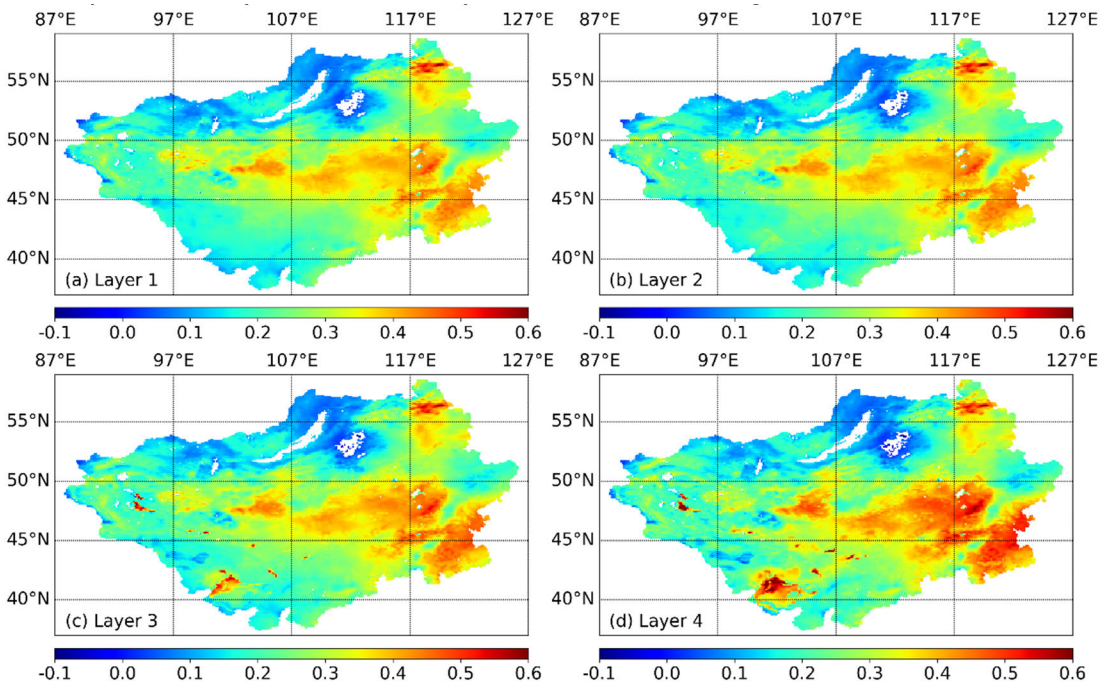

FIGURE 20. Spatial evolutionary trend of different ST layers on the MP. Areas without significant trends are shown in white.

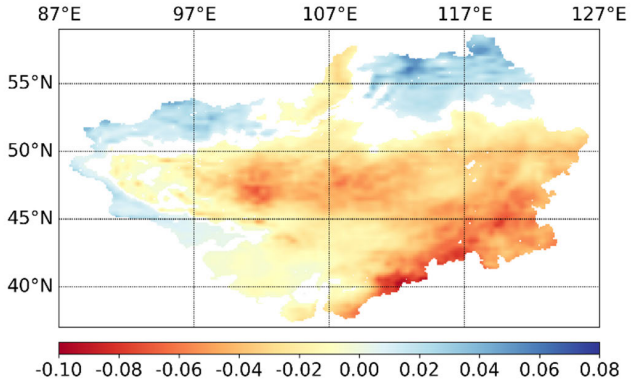

FIGURE 21. Spatial evolutionary trend of precipitation in the MP. Areas without significant trends are shown in white.

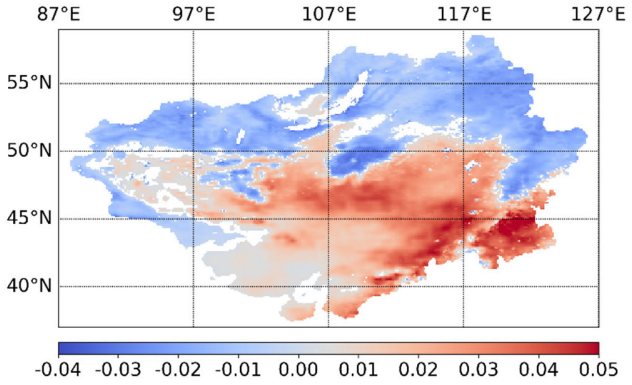

FIGURE 22. Spatial evolutionary trend of evaporation in MP. Areas without significant trends are shown in white.

C. UNCERTAINTIES

The results derived from our study were mainly based on the ERA5-Land monthly averaged products. Great efforts have been devoted to evaluating the accuracy of ERA5-Land products, and ERA5-Land has shown favorable performance compared to its predecessors as well as other reanalysis products [19], [28], [60]. However, the multi-depth SM, ST, precipitation, and evaporation dataset are derived from the ERA5-Land products, which means inborn uniformity among these datasets. In-depth investigation using mutually independent datasets is expected in future to explore the evolution pattern of SM under the influences of climatic factors.

Additionally, diversified uncertainties inevitably exist in the ERA5-Land assimilation processes, leading to certain instabilities both spatially and temporally. For instance, Xin *et al.* [61] found that further improvement could be essential for ERA5-Land products to provide accurate precipitation patterns in areas with high urbanization levels. Wu *et al.* [30] thoroughly validated the ERA5-Land SM in China and revealed that the performance of the ERA5-Land SM was mostly determined by SM climatology. In particular, the ERA5-Land SM expressed a relatively large bias in humid and semi-humid areas. In addition to ST, precipitation, and evaporation, many other factors (i.e., soil texture, groundwater depth, and vegetation) could also affect the distribution patterns of SM. As a classical measurement method, the Granger causality test has been widely accepted and used in Earth system science studies. However, it may not be sufficiently rigorous to define a temporal-related phenomenon as

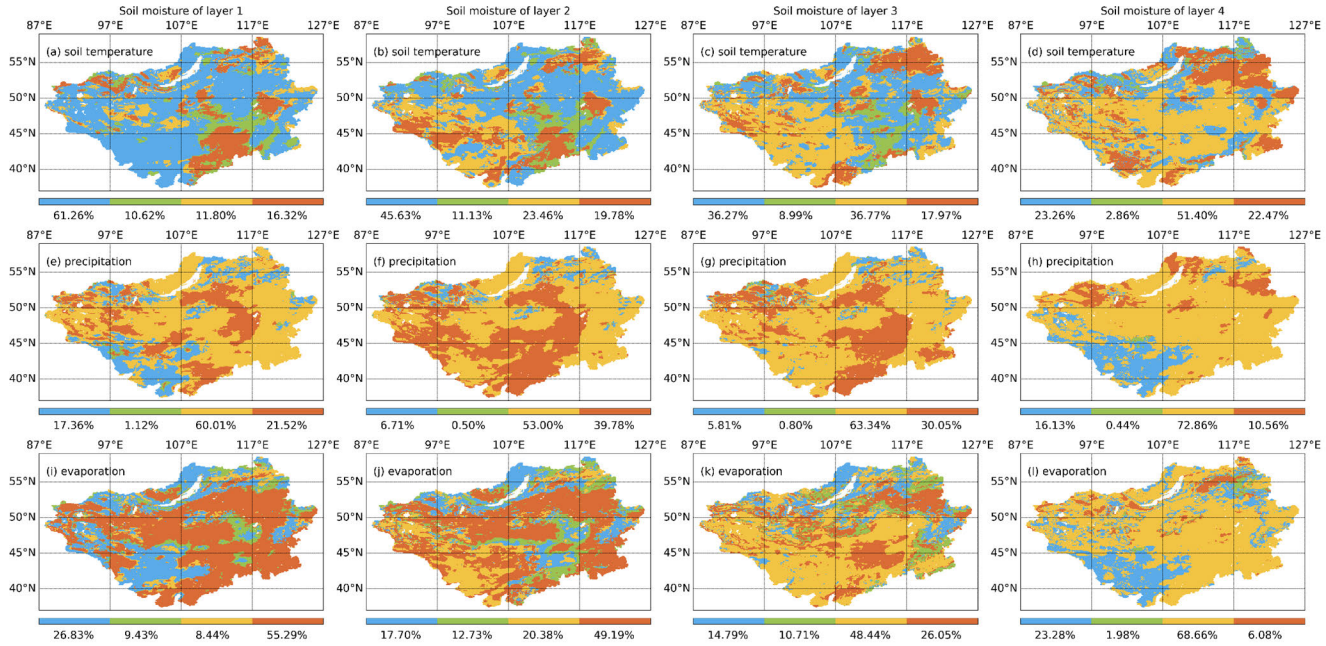

FIGURE 23. Granger causality between ST ((a)–(d)), precipitation ((e)–(h)), evaporation ((i)–(l)), and corresponding SM. The red areas are identified with bidirectional causality relationships between the SM and the related climate parameters; the yellow indicates that the related climate parameters are the unidirectional cause of the SM, and the green indicates that the SM is the unidirectional cause of the related climate parameters. Areas without significant causal links are shown in blue.

causality. Therefore, this study conducted a causality analysis to attempt to explain the reason for the increase in SM variation.

In addition to climatic factors, the variability of SM can also be directly or indirectly affected by human activities, such as domestic water withdrawal, livestock, irrigation, mining, electricity, and manufacturing. With the steady growth of population and economic development, an equal increase in human water use intensity can influence the sustainable soil water resource supply [62], [63]. Therefore, it is primarily assumed that the fluctuation in SM is a comprehensive expression jointly driven by both climatic and human factors. Future studies should focus on the duration, intensity, and pattern of artificial interference in SM variations.

V. CONCLUSION

In summary, this study preliminarily confirmed the trend of SM loss in the MP from 1950 to 2020 using reanalysis products. Specifically, as the depth increased, the drying trend was notably aggravated at the same time (-0.003 m^3/m^3 per decade for 0–7 cm depth and -0.005 m^3/m^3 per decade for 100–289 cm depth), suggesting that the available soil water content for vegetation roots would decrease. Additionally, the seasonal dynamics of deep-layer SM could be less volatile than those of surface-layer SM because of the interception of surface-layer SM to atmospheric conditions. Through Granger causality analysis, precipitation was found to be the predominant reason for the efficient variation in SM across different depths during the warm period (ST>0 °C). Simultaneously, a pre-existing response of the SM to precipitation was observed. Moreover, the evaporation and land surface SM displayed close interactions, and this bidirectional interactive response turned unidirectional (the impact of deep layer SM on evaporation remarkably decreased) with increasing depth during the warm period (ST>0 °C). The interaction analysis was expected to improve the understanding of the spatial and temporal SM dynamics in the MP. However, this study merely conducted a preliminary investigation of the evolutionary characteristics of SM fluctuations under the background of global climate warming. In particular, more in-depth analysis devoted to exploring the intrinsic mechanism of SM change is necessary in the future.

ACKNOWLEDGMENT

The authors would like to thank the anonymous reviewers for their insightful comments on this study.

REFERENCES

[1] D. A. Robinson, C. S. Campbell, J. W. Hopmans, B. K. Hornbuckle, S. B. Jones, R. Knight, F. Ogden, J. Selker, and O. Wendroth, "Soil moisture measurement for ecological and hydrological watershed-scale observatories: A review," *Vadose Zone J.*, vol. 7, pp. 358–389, Feb. 2008.

[2] R. H. Reichle, R. D. Koster, J. Dong, and A. A. Berg, "Global soil moisture from satellite observations, land surface models, and ground data: Implications for data assimilation," *J. Hydrometeorol.*, vol. 5, no. 3, pp. 430–442, 2009.

[3] S. I. Seneviratne, T. Corti, E. L. Davin, M. Hirschi, E. B. Jaeger, I. Lehner, B. Orlowsky, and A. J. Teuling, "Investigating soil moisture–climate interactions in a changing climate: A review," *Earth-Sci. Rev.*, vol. 99, nos. 3–4, pp. 125–161, 2010.

[4] Y. Liu, Y. Zhou, N. Lu, R. Tang, N. Liu, Y. Li, J. Yang, W. Jing, and C. Zhou, "Comprehensive assessment of Fengyun-3 satellites derived soil moisture with *in-situ* measurements across the globe," *J. Hydrol.*, vol. 594, Mar. 2021, Art. no. 125949.

[5] Y. Liu, W. Jing, S. Sun, and C. Wang, "Multi-scale and multi-depth validation of soil moisture from the China land data assimilation system," *IEEE J. Sel. Topics Appl. Earth Observ. Remote Sens.*, vol. 14, pp. 9913–9930, 2021.

[6] N. Pan, S. Wang, Y. Liu, W. Zhao, and B. Fu, "Global surface soil moisture dynamics in 1979–2016 observed from ESA CCI SM dataset," *Water*, vol. 11, no. 5, p. 883, Apr. 2019.

[7] I. E. Mladenova, "Evaluating the operational application of SMAP for global agricultural drought monitoring," *IEEE J. Sel. Topics Appl. Earth Observ. Remote Sens.*, vol. 12, no. 9, pp. 3387–3397, Sep. 2019.

[8] L. Yang, G. Sun, L. Zhi, and J. Zhao, "Negative soil moisture-precipitation feedback in dry and wet regions," *Sci. Rep.*, vol. 8, no. 1, p. 4026, Dec. 2018.

[9] Y. Deng, S. Wang, X. Bai, G. Luo, L. Wu, Y. Cao, H. Li, C. Li, Y. Yang, Z. Hu, and S. Tian, "Variation trend of global soil moisture and its cause analysis," *Ecol. Indicators*, vol. 110, Mar. 2020, Art. no. 105939.

[10] J. Sheffield and E. F. Wood, "Global trends and variability in soil moisture and drought characteristics, 1950–2000, from observation-driven simulations of the terrestrial hydrologic cycle," *J. Climate*, vol. 21, no. 3, pp. 432–458, Feb. 2008.

[11] C. Albergel *et al.*, "Skill and global trend analysis of soil moisture from reanalyses and microwave remote sensing," *J. Hydrometeorol.*, vol. 14, no. 4, pp. 1259–1277, 2013.

[12] G. Bao, Z. Qin, Y. Bao, Y. Zhou, W. Li, and A. Sanjjav, "NDVI-based long-term vegetation dynamics and its response to climatic change in the Mongolian Plateau," *Remote Sens.*, vol. 6, no. 9, pp. 8337–8358, Sep. 2014.

[13] R. Hassan, R. Scholes, and N. Ash, *Ecosystems and Human Well-Being: Current State and Trends*. Washington, DC, USA: Island Press, 2005.

[14] H. Jiang, N. Lu, X. Zhang, L. Yao, and Y. Bai, "Satellite observed cooling effects from re-vegetation on the Mongolian Plateau," *Sci. Total Environ.*, vol. 781, Aug. 2021, Art. no. 146707.

[15] S. Tao, "Rapid loss of lakes on the Mongolian Plateau," in *Proc. PNAS*, 2015, vol. 112, no. 7, pp. 2281–2286.

[16] R. John, J. Chen, Z.-T. Ou-Yang, J. Xiao, R. Becker, A. Samanta, S. Ganguly, W. Yuan, and O. Batkhishig, "Vegetation response to extreme climate events on the Mongolian plateau from 2000 to 2010," *Environ. Res. Lett.*, vol. 8, no. 3, Sep. 2013, Art. no. 035033.

[17] Y. Liu, Q. Zhuang, M. Chen, Z. Pan, N. Tchebakova, A. Sokolov, D. Kicklighter, J. Melillo, A. Sirin, G. Zhou, Y. He, J. Chen, L. Bowling, D. Miralles, and E. Parfenova, "Response of evapotranspiration and water availability to changing climate and land cover on the Mongolian Plateau during the 21st century," *Global Planet. Change*, vol. 108, pp. 85–99, Sep. 2013.

[18] S. Bontemps, P. Defourny, J. Radoux, E. Van Bogaert, C. Lamarche, F. Achard, P. Mayaux, M. Boettcher, C. Brockmann, G. Kirches, M. Zülkhe, V. Kalogirou, F. M. Seifert, and O. Arino, "Consistent global land cover maps for climate modelling communities: Current achievements of the ESA's land cover CCI," in *Proc. ESA Living Planet Symp.*, Edimburgh, 2013, pp. 1–6.

[19] H. Hersbach, B. Bell, P. Berrisford, S. Hirahara, A. Horányi, J. Muñoz-Sabater, J. Nicolas, C. Peubey, R. Radu, D. Schepers, and A. Simmons, "The ERA5 global reanalysis," *Quart. J. Roy. Meteorol. Soc.*, vol. 146, no. 730, pp. 1999–2049, Jul. 2020.

[20] L. Hoffmann, D. Li, O. Stein, X. Wu, S. Griessbach, Y. Heng, P. Konopka, R. Müller, B. Vogel, and J. S. Wright, "From ERA-interim to ERA5: The considerable impact of ECMWF's next-generation reanalysis on Lagrangian transport simulations," *Atmos. Chem. Phys.*, vol. 19, no. 5, pp. 3097–3124, Mar. 2019.

[21] A. Shrestha, A. S. Nair, and J. Indu, "Role of precipitation forcing on the uncertainty of land surface model simulated soil moisture estimates," *J. Hydrol.*, vol. 580, Jan. 2020, Art. no. 124264.

[22] J. Qiu, Q. Gao, S. Wang, and Z. Su, "Comparison of temporal trends from multiple soil moisture data sets and precipitation: The implication of irrigation on regional soil moisture trend," *Int. J. Appl. Earth Observ. Geoinf.*, vol. 48, pp. 17–27, Jun. 2016.

[23] S. Tuttle and G. Salvucci, "Empirical evidence of contrasting soil moisture–precipitation feedbacks across the United States," *Science*, vol. 352, no. 6287, pp. 825–828, May 2016.

[24] M. E. Holzman, R. Rivas, and M. C. Piccolo, "Estimating soil moisture and the relationship with crop yield using surface temperature and vegetation index," *Int. J. Appl. Earth Observ. Geoinformation*, vol. 28, pp. 181–192, May 2014.

[25] I. Sandholt, K. Rasmussen, and J. Andersen, "A simple interpretation of the surface temperature/vegetation index space for assessment of surface moisture status," *Remote Sens. Environ.*, vol. 79, pp. 213–224, Feb. 2002.

[26] T. L. Delworth and S. Manabe, "The influence of potential evaporation on the variabilities of simulated soil wetness and climate," *J. Climate*, vol. 1, no. 5, pp. 523–547, May 1988.

[27] V. Mishra, W. L. Ellenburg, R. E. Griffin, J. R. Mecikalski, J. F. Cruise, C. R. Hain, and M. C. Anderson, "An initial assessment of a SMAP soil moisture disaggregation scheme using TIR surface evaporation data over the continental United States," *Int. J. Appl. Earth Observ. Geoinf.*, vol. 68, pp. 92–104, Jun. 2018.

[28] M. Li, P. Wu, and Z. Ma, "A comprehensive evaluation of soil moisture and soil temperature from third-generation atmospheric and land reanalysis data sets," *Int. J. Climatol.*, vol. 40, no. 13, pp. 5744–5766, Nov. 2020.

[29] M. Cheng, L. Zhong, Y. Ma, M. Zou, N. Ge, X. Wang, and Y. Hu, "A study on the assessment of multi-source satellite soil moisture products and reanalysis data for the Tibetan Plateau," *Remote Sens.*, vol. 11, no. 10, p. 1196, May 2019.

[30] Z. Wu, H. Feng, H. He, J. Zhou, and Y. Zhang, "Evaluation of soil moisture climatology and anomaly components derived from ERA5-land and GLDAS-2.1 in China," *Water Resour. Manage.*, vol. 35, no. 2, pp. 629–643, Jan. 2021.

[31] C. O. Justice *et al.*, "The Moderate Resolution Imaging Spectroradiometer (MODIS): Land remote sensing for global change research," *IEEE Trans. Geosci. Remote Sens.*, vol. GRS-36, no. 4, pp. 1228–1249, Jul. 1988.

[32] S. Shekhar, H. Xiong, and X. Zhou, "GDAL," in *Encyclopedia of GIS*, S. Shekhar, H. Xiong, and X. Zhou, Eds. Cham, Switzerland: Springer, 2017, p. 644.

[33] P. C. Spennemann, J. A. Rivera, A. C. Saulo, and O. C. Penalba, "A comparison of GLDAS soil moisture anomalies against standardized precipitation index and multisatellite estimations over south America," *J. Hydrometeorol.*, vol. 16, no. 1, pp. 158–171, Feb. 2015.

[34] E. Zivot and J. Wang, "Rolling analysis of time series," in *Modeling Financial Time Series With S-Plus®*. New York, NY, USA: Springer, 2003, pp. 299–346.

[35] C. W. Granger, "Investigating causal relations by econometric models and cross-spectral methods," *Econometrica, J. Econ. Soc.*, vol. 37, no. 3, 1969, pp. 424–438.

[36] M. Ding, Y. Chen, and S. Bressler, "Granger causality: Basic theory and application to neuroscience," in *Handbook of Time Series Analysis: Recent Theoretical Developments Applications*. Weinheim, Germany: Wiley, 2006, p. 437.

[37] J. R. Freeman, "Granger causality and the times series analysis of political relationships," *Amer. J. Political Sci.*, vol. 27, no. 2, pp. 327–358, May 1983.

[38] A. Dutta, "Telecommunications and economic activity: An analysis of Granger causality," *J. Manage. Inf. Syst.*, vol. 17, no. 4, pp. 71–95, 2001.

[39] J. Runge, S. Bathiany, E. Bollt, G. Camps-Valls, D. Coumou, E. Deyle, C. Glymour, M. Kretschmer, M. D. Mahecha, J. Muñoz-Marí, E. H. van Nes, J. Peters, R. Quax, M. Reichstein, M. Scheffer, B. Schölkopf, P. Spirtes, G. Sugihara, J. Sun, K. Zhang, and J. Zscheischler, "Inferring causation from time series in Earth system sciences," *Nature Commun.*, vol. 10, no. 1, pp. 1–13, Dec. 2019.

[40] C. Papagiannopoulou, D. G. Miralles, S. Decubber, M. Demuzere, N. E. C. Verhoest, W. A. Dorigo, and W. Waegeman "A non-linear Granger-causality framework to investigate climate-vegetation dynamics," *Geosci. Model Develop.*, vol. 10, no. 5, pp. 1945–1960, 2017.

[41] B. Jiang, S. Liang, and W. Yuan, "Observational evidence for impacts of vegetation change on local surface climate over northern China using the Granger causality test," *J. Geophys. Research, Biogeosciences*, vol. 120, no. 1, pp. 1–12, Jan. 2015.

[42] D. Kong, C. Miao, Q. Duan, X. Lei, and H. Li, "Vegetation-climate interactions on the Loess Plateau: A nonlinear Granger causality analysis," *J. Geophys. Res., Atmos.*, vol. 123, no. 19, pp. 68–79, 2018.

[43] M. Mirzargar, R. T. Whitaker, and R. M. Kirby, "Curve boxplot: Generalization of boxplot for ensembles of curves," *IEEE Trans. Vis. Comput. Graphics*, vol. 20, no. 12, pp. 2654–2663, Dec. 2014.

[44] F. Meng, M. Luo, C. Sa, M. Wang, and Y. Bao, "Quantitative assessment of the effects of climate, vegetation, soil and groundwater on soil moisture spatiotemporal variability in the Mongolian Plateau," *Sci. Total Environ.*, vol. 809, Feb. 2022, Art. no. 152198.

[45] M. Luo, C. Sa, F. Meng, Y. Duan, T. Liu, and Y. Bao, "Assessing remotely sensed and reanalysis products in characterizing surface soil moisture in the Mongolian Plateau," *Int. J. Digit. Earth*, vol. 14, no. 10, pp. 1255–1272, Oct. 2021.

[46] B. Martens, D. G. Miralles, H. Lievens, R. van der Schalie, R. A. M. de Jeu, D. Fernández-Prieto, H. E. Beck, W. A. Dorigo, and N. E. C. Verhoest, "GLEAM V3: Satellite-based land evaporation and root-zone soil moisture," *Geosci. Model Develop. Discuss.*, vol. 10, no. 5, pp. 1–36, 2017.
[47] P. A. Dirmeyer, C. A. Schlosser, and K. L. Brubaker, "Precipitation, recycling, and land memory: An integrated analysis," *J. Hydrometeorol.*, vol. 10, no. 1, pp. 278–288, Feb. 2009.
[48] R. D. Koster, P. A. Dirmeyer, Z. Guo, G. Bonan, and E. Chan, "Regions of strong coupling between soil moisture and precipitation," *Science*, vol. 305, no. 5687, pp. 40–1138, 2004.
[49] F. Mohseni and M. Mokhtarzade, "A new soil moisture index driven from an adapted long-term temperature-vegetation scatter plot using MODIS data," *J. Hydrol.*, vol. 581, Feb. 2020, Art. no. 124420.
[50] H. Wouters, J. Keune, I. Y. Petrova, C. C. van Heerwaarden, A. J. Teuling, J. S. Pal, J. V.-G. de Arellano, and D. G. Miralles, "Soil drought can mitigate deadly heat stress thanks to a reduction of air humidity," *Sci. Adv.*, vol. 8, no. 1, 2022, Art. no. eabe6653.
[51] H.-C. Zuo, "Observation and numerical simulation of heterogenous underlying surface boundary layer (I): The whole physical picture of cold island effect and inverse humidity," *Plateau Meteorol.*, vol. 23, no. 2, pp. 155–162, 2004.
[52] J. Pellenq, J. Kalma, G. Boulet, and G. M. Saulnier, "A disaggregation scheme for soil moisture based on topography and soil depth," *J. Hydrol.*, vol. 276, nos. 1–4, pp. 112–127, May 2003.
[53] H. J. Tromp-van Meerveld and J. J. McDonnell, "On the interrelations between topography, soil depth, soil moisture, transpiration rates and species distribution at the hillslope scale," *Adv. Water Resour.*, vol. 29, no. 2, pp. 293–310, Feb. 2006.
[54] H. Davarzani, K. Smits, R. M. Tolene, and T. Illangasekare, "Study of the effect of wind speed on evaporation from soil through integrated modeling of the atmospheric boundary layer and shallow subsurface," *Water Resour. Res.*, vol. 50, no. 1, pp. 661–680, Jan. 2014.
[55] H. F. Cook, "Mulch effects on rainfall interception, soil physical characteristics and temperature under *Zea mays L.*," *Soil Tillage Res.*, vol. 91, nos. 1–2, pp. 227–235, 2006.
[56] Z. Xing, L. Fan, L. Zhao, G. De Lannoy, F. Frappart, J. Peng, X. Li, J. Zeng, A. Al-Yaari, K. Yang, T. Zhao, J. Shi, M. Wang, X. Liu, G. Hu, Y. Xiao, E. Du, R. Li, and J.-P. Wigneron, "A first assessment of satellite and reanalysis estimates of surface and root-zone soil moisture over the permafrost region of Qinghai-Tibet plateau," *Remote Sens. Environ.*, vol. 265, Nov. 2021, Art. no. 112666.
[57] T. P. Anguela, M. Zribi, S. Hasenauer, F. Habets, and C. Loumagne, "Analysis of surface and root-zone soil moisture dynamics with ERS scatterometer and the hydrometeorological model SAFRAN-ISBA-MODCOU at grand morin watershed (France)," *Hydrol. Earth Syst. Sci.*, vol. 12, no. 6, pp. 1415–1424, Dec. 2008.
[58] M. Hirschi, B. Mueller, W. Dorigo, and S. I. Seneviratne, "Using remotely sensed soil moisture for land–atmosphere coupling diagnostics: The role of surface vs. root-zone soil moisture variability," *Remote Sens. Environ.*, vol. 154, pp. 246–252, Nov. 2014.
[59] A. W. Al-Kayssi, A. A. Al-Karaghouli, A. M. Hasson, and S. A. Beker, "Influence of soil moisture content on soil temperature and heat storage under greenhouse conditions," *J. Agricult. Eng. Res.*, vol. 45, pp. 241–252, Jan. 1990.
[60] S. S. Mahto and V. Mishra, "Does ERA-5 outperform other reanalysis products for hydrologic applications in India?" *J. Geophys. Research, Atmos.*, vol. 124, no. 16, pp. 9423–9441, Aug. 2019.
[61] Y. Xin, N. Lu, H. Jiang, Y. Liu, and L. Yao, "Performance of ERA5 reanalysis precipitation products in the Guangdong-Hong Kong-Macao greater bay area, China," *J. Hydrol.*, vol. 602, Nov. 2021, Art. no. 126791.
[62] A. Puy, E. Borgonovo, S. Lo Piano, S. A. Levin, and A. Saltelli, "Irrigated areas drive irrigation water withdrawals," *Nature Commun.*, vol. 12, no. 1, pp. 1–12, Dec. 2021.
[63] P. D. Colaizzi, E. M. Barnes, T. R. Clarke, C. Y. Choi, and P. M. Waller, "Estimating soil moisture under low frequency surface irrigation using crop water stress index," *J. Irrigation Drainage Eng.*, vol. 129, no. 1, pp. 27–35, Feb. 2003.

YANGXIAOYUE LIU received the B.S. degree in geography science from Shandong Normal University, Jinan, China, in 2013, the M.S. degree in cartography and geographical information system from the Shandong University of Science and Technology, Qingdao, China, in 2016, and the Ph.D. degree in cartography and geographical information system from the State Key Laboratory of Resources and Environmental Information System, Institute of Geographic Sciences and Natural Resources Research (IGSNRR), Chinese Academy of Sciences (CAS), Beijing, China, in 2019. She is currently an Assistant Research Fellow with IGSNRR. Her research interests include satellite-based environment remote sensing and spatio-temporal data mining.

YAPING YANG is a Senior Engineer of the Institute of Geographic Sciences and Natural Resources Research (IGSNRR), Chinese Academy of Sciences (CAS), the Director of the National Earth System Science Data Center, the Deputy Director of the Research Laboratory of Earth Data Science and Sharing of IGSNRR, the Director of the Earth System Science Data Center of CAS, a Person-in-Charge of the Geography Resources and Ecology Knowledge Service System of China Knowledge Center for Engineering Sciences and Technology, and a Person-in-Charge of the Data Collection and Delivery Management Center for the National Key Basic Research and Development Plan (973 Projects) in the field of resources and environment for the National Science and Technology Basic Resources Investigation Projects. She has been engaged in the research and practice of earth data science and informatization in scientific researches.